Shi et al. Heritage Science (2024) 12:178
https://doi.org/10.1186/s40494-024-01296-0

Heritage Science

RESEARCH Open Access

Water vapor condensation prevention and risk rating evaluation based on Yang Can's tomb

Wentao Shi[1], Ping Liu[1*], Bo Sun[1,2,3], Qian Wang[1], Xiaokun Xie[1], Yuyuan Liang[3] and Changqing Li[3]

Abstract

Temperature and humidity variations in burial stone relics can easily cause water vapor condensation, which is an important factor leading to their deterioration. However, the water vapor condensation mechanism and the evaluation of risk ratings have always been difficult problems in the protection of cultural relics. In this study, the water vapor condensation mechanism in Yang Can's tomb was comprehensively investigated through on-site monitoring, indoor experiments and software simulations, on the basis of which a physical model of water vapor condensation in this tomb was established and a water vapor condensation risk rating assessment method was proposed. The proposed method considers the difference between the dew point and wall temperatures within the tomb (dew–wall temperature difference) and the duration of water vapor condensation, and corresponding preventive and control measures were formulated for different risk ratings. The study revealed that when the wall temperature of the chamber is lower than the dew point temperature, water vapor starts to condense. The larger the dew–wall temperature difference is, the greater the risk of condensation. In addition, specific water vapor condensation prevention and control measures were proposed for Yang Can's tomb, and the prevention and control effects were simulated. The simulation results showed that favorable prevention and control effects could be achieved, and the proposed measures could be applied in practice. This study holds notable significance for investigating the water vapor condensation mechanism and evaluating the risk ratings of burial stone relics and provides a theoretical basis and reference for water vapor condensation prevention and control in burial stone relics.

Keywords Burial stone relics, Heritage conservation, Water vapor condensation, Risk rating assessment, Simulation analysis

Introduction

Among the known tombs of the Song Dynasty in Southwest China, Yang Can's tomb is the largest. Yang Can's tomb was built during the Song Dynasty (1241–1252) and has a history of more than 700 years. Yang Can's tomb is located in Huangfenzui, approximately 10 km southeast of Zunyi city, Guizhou Province (Fig. 1a), which is the second batch of national key cultural relic protection units in China. The tomb chamber is constructed of white sandstone (Fig. 1b), and the indoor area is approximately 50 m^2 [1]. Yang Can's tomb is located in Southwest China, which exhibits a

*Correspondence:
Ping Liu
liuping@lzu.edu.cn
[1] Key Laboratory of Mechanics on Disaster and Environment in Western China, College of Civil Engineering and Mechanics, Lanzhou University, Lanzhou 730000, China
[2] China Railway Cultural Heritage Rehabilitation Technology Innovation Co., Ltd. of China Railway Engineering Corporation, Lanzhou 730000, China
[3] School of Civil Engineering, Lanzhou University of Technology, Lanzhou 730050, China

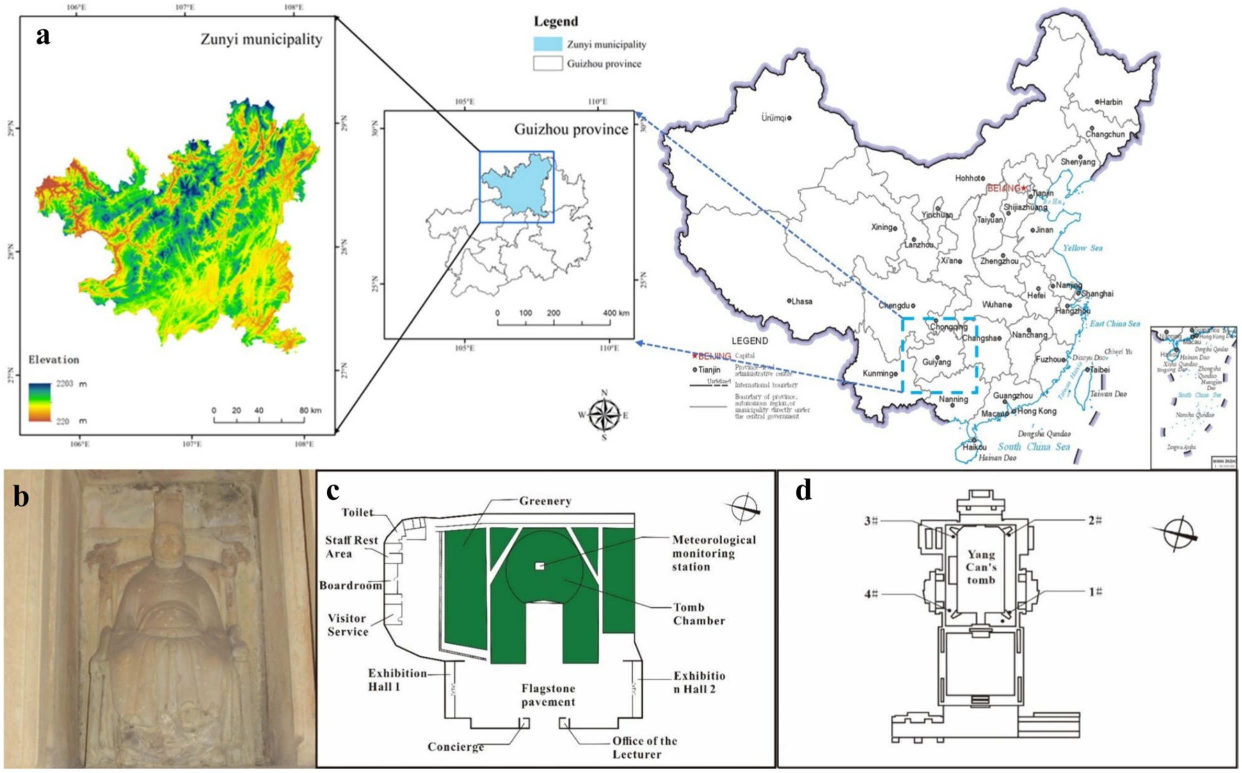

Fig. 1 Overview map of the study area: **a** Location and topography of Yang Can's tomb; **b** stone statue of the male host of Yang Can's tomb; **c** plan view of Yang Can's tomb **d** distribution of the survey points inside the chamber

subtropical monsoon humid climate, and the annual rainfall is high. Hence, the tomb exhibits a year-round humid, semienclosed environment (Fig. 1c). Therefore, the severity of the weathering problems caused by water seepage is increasing. At present, problems due to atmospheric precipitation and capillary water infiltration have been effectively solved in existing protection projects (Fig. 2b). However, the problems associated with the weathering of stone carvings in tombs due to water vapor condensation must still be addressed (Fig. 2c). Due to the increasing damage caused by water condensation in Yang Can's tomb, the risks of damage and destruction

Fig. 2 Yang Can's tomb: **a** Stone carvings in the tomb; **b** water seepage disease in the tomb; **c** weathering disease of the stone carvings

of cultural relics are very high, and corresponding management measures are urgently needed. First, the water condensation mechanism should be studied, and corresponding protection measures should be proposed.

The study of water vapor condensation can be traced back to the mid-19 century. Research during that period focused on condensate generation and the factors influencing the amount of condensate generated. Reynolds and Roscoe [2] proposed that a cold surface can be enveloped by air to impede the condensation process. The concept of water vapor condensation was first proposed by Monteith [3], who considered water vapor condensation a phenomenon in which the atmospheric temperature around a given feature decreases below the dew point temperature, thereby producing condensation water. The process of condensate formation and disappearance actually entails the mutual transformation of condensation and evaporation processes [4]. Factors such as the wind speed, temperature, precipitation and humidity affect the amount of condensation water generated [5, 6].

Research on water vapor condensation in the field of heritage conservation can be traced back to the 20th century. Moreover, water vapor condensation research during that period mainly focused on ancient aboveground building sites [7–11]. Mahdavinejad et al. [12], by analyzing a series of problems caused by condensation in historic buildings, proposed a method to reduce the possibility of condensation by reducing the temperature difference through active ventilation. Franzoni et al. [13] investigated the effect of mortar joints on capillary rise rates. Condensation plays an important role in castle stone degradation [14]. Subsequent studies began to focus on monitoring water transport at cultural heritage sites [15–20]. These studies provided valuable information for stone cultural heritage preservation. With the development of science and technology, numerical simulations are increasingly used for studying condensation [21–30]. Water plays a crucial role in the degradation and conservation of architectural and rock-cut heritage structures [31, 32]. Huang et al. [33] concluded that natural moisture condensation is an important factor contributing to the weathering of stone artifacts. If conservation efforts focused only on the conditions under which water forms at the surface, this could lead to the repeated formation of liquid water inside stone artifacts, which could cause considerable damage to the remaining stone. This conclusion provides helpful guidance for eliminating the harmful effects of water condensation. With increasing research, the number of studies on the mechanism of seepage defects has increased [34–40], and an increasing number of conservation measures for cultural relics have been proposed [41–48]. These arguments are important for subsequent research and prevention of water condensation in stone cultural relics, but there is still a lack of relevant research focused on assessing the risk of water vapor condensation on the surface of stone artifacts.

This research aimed to investigate the water vapor condensation mechanism and to formulate preventive measures for burial stone relics. Based on the protection plan of Yang Can's tomb to solve the problems of cultural relics under the influence of the environment, combined with the lack of research on protection against water condensation in the sandstone surface layer of Yang Can's tomb, the water vapor condensation mechanism in Yang Can's tomb was investigated from three aspects: on-site inspection, indoor testing and software simulations. Considering the duration of water vapor condensation, a water vapor condensation risk assessment method for burial stone relics was proposed. In addition, measures for preventing water vapor condensation in Yang Can's tomb were formulated, and the prevention and control effects were simulated and analyzed. This study could provide a sound basis for preventing and controlling water condensation in Yang Can's tomb. Moreover, this study could offer a reference and new arguments for risk assessment of water vapor condensation in burial stone relics.

Field monitoring, indoor tests and software simulations

Field monitoring

Monitoring instrument

In this paper, with reference to previous studies [49], an infrared thermal imager was selected to measure the wall temperature of the chamber of Yang Can's tomb. The test was conducted using a TiX560 infrared thermal imager (Fig. 3), which provides a temperature measurement range of − 20 to 1200 °C and a measurement accuracy of up to ± 2 °C or 2% at 25 °C, with an emissivity of 0.68.

Monitoring method

The arrangement of the environmental parameter monitoring points in the crypt is shown in Fig. 1d. At measurement points #1–#4, automatic temperature and humidity recorders were installed, and the measurement data were input on the monitoring computer platform through an automatic acquisition system. Moreover, the data were collected at 30 min intervals, while

Fig. 3 FLUKE Tix560 thermal imaging camera

environmental parameter data were continuously recorded for one year.

In this paper, the wall temperature inside the chamber of Yang Can's tomb was monitored by an infrared thermal imager on two typical days in March, and the obtained data basically represented the temperature variations of the wall surface of Yang Can's tomb. The monitoring frequency was once every 2 hours, with 48 h of continuous monitoring. The monitoring objects at different depths of the wall inside the chamber were recorded with an infrared camera installed at a distance of 2 m from the wall to reduce human errors during the temperature measurements. It was also ensured that the monitoring period did not exceed five minutes to eliminate variations in the environment within the chamber due to human factors as much as possible.

After field monitoring with the FLUKE Tix560 infrared thermal imager, thermal imaging analysis and processing software FLUKE SmartView was employed to read and process the temperature data of the chamber walls, and the average values were selected for analysis and comparison in this paper. A comparison of the infrared thermographic image of Yang Can's tomb recorded at 13:40 on 8 March 2023 with a visible light image is shown in Fig. 4.

Indoor test

Sandstone density test

In this paper, the wax sealing method was chosen to measure the density of sandstone in Yang Can's tomb.

Moisture absorption test

In this paper, the moisture absorption test method was applied to determine the equilibrium moisture content in sandstone at 20 ℃ under different air relative humidity conditions (Fig. 5a). The selected saturated salt solutions are listed in Table 1.

Water vapor permeability coefficient test

Experimental studies have shown that the effect of temperature variations on the water vapor permeability coefficient is limited and can be neglected [50]. Therefore, the effect of temperature was not considered in this paper. In this paper, the water vapor permeability coefficient of specimens was measured by the desiccant method (Fig. 5b).

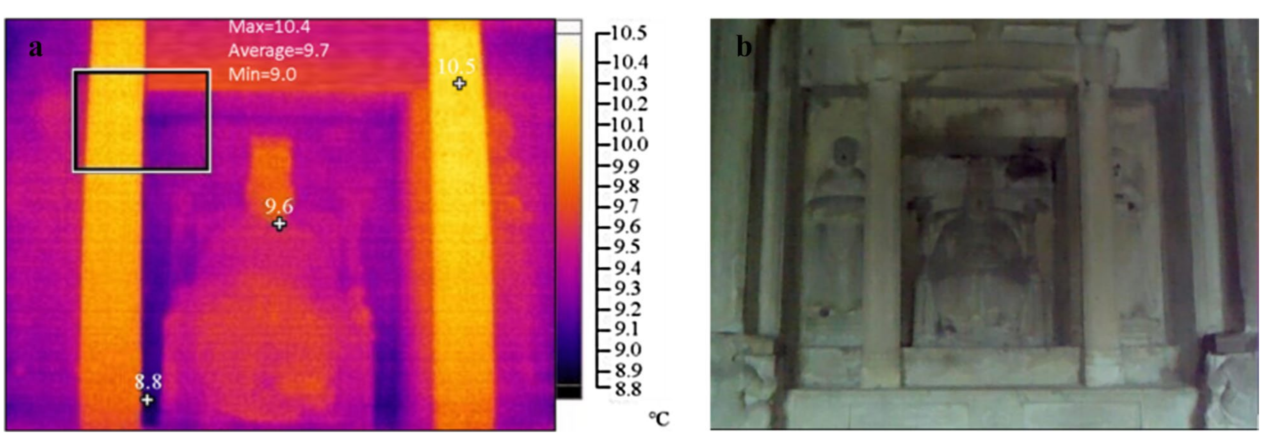

Fig. 4 Comparison of infrared thermographic and visible light images: **a** Infrared thermographic image; **b** visible light image

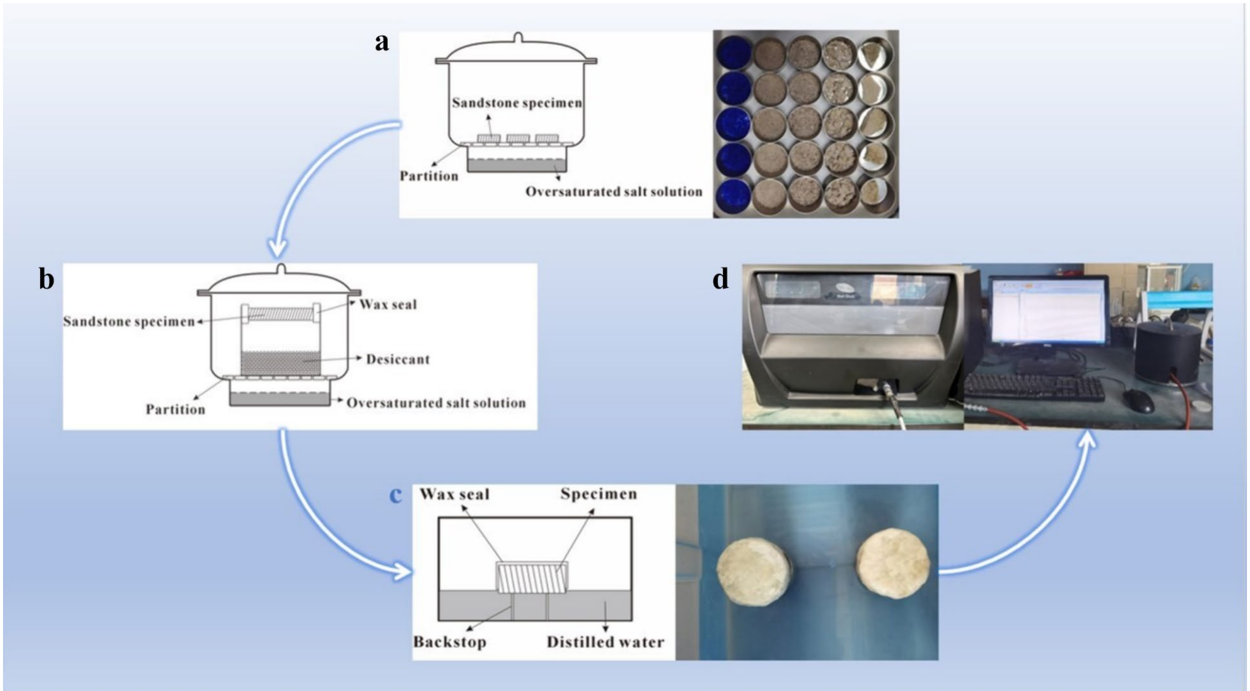

Fig. 5 Diagram of the indoor tests: **a** Moisture absorption test; **b** water vapor permeability coefficient test; **c** liquid water diffusion coefficient test; **d** thermal conductivity test

Table 1 Relative humidity of the saturated salt solution at 20 °C

Saturated salt solution	Relative air humidity (%)
$MgCl_2$	33.1 ± 0.2
K_2CO_3	43.2 ± 0.4
NaBr	59.14 ± 0.44
NaCl	75.5 ± 0.2
K_2SO_4	97.6 ± 0.6

Liquid water diffusion coefficient test

The ability to transfer liquid water can be represented by the liquid water transfer coefficient. In this paper, the specimens were immersed on one side to measure the liquid water transfer coefficient in accordance with the international standard ISO 15148:2002(E). The test device used is shown in Fig. 5c.

Thermal conductivity test

The thermal conductivity and thermal diffusion coefficient of the specimens were measured by a thermal constant analyzer [51] (model: Hot disk TPS2500s, Fig. 5d).

Software simulation

In this paper, numerical simulations were performed using COMSOL Multiphysics software. For stone cultural relics, the use of simulation software could limit the destruction and damage caused by human factors. We referred to our previous study [52] and adopted the established model and parameters to simulate the interior environment of the chamber.

Monitoring, testing and simulation results

Monitoring results

Monitoring data for the year

Temperature Figure 6 shows the air temperature variations at measurement points #1 and #2 inside the chamber of the Yang Can tomb. A portion of the meteorological data from April to early May was lost due to equipment system upgrades. The trend was similar between the two sites. However, the temperatures at different depths slightly varied from season to season.

Relative humidity In summer, the relative humidity inside the chamber is already high, and coupled with the fact that the wind speed in summer is lower than that during the other seasons, the air circulation at large depths within the chamber is more difficult than that at shallower depths. Thus, the relative humidity difference in summer between shallow and deep points is greater (Fig. 7).

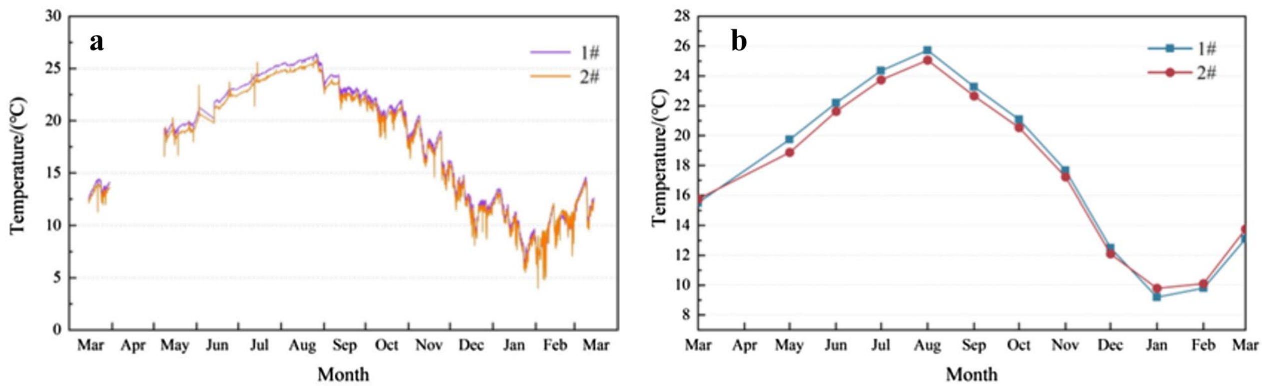

Fig. 6 Temperature variations at the different measurement points: **a** Temperature variations throughout one year; **b** monthly average temperature variations

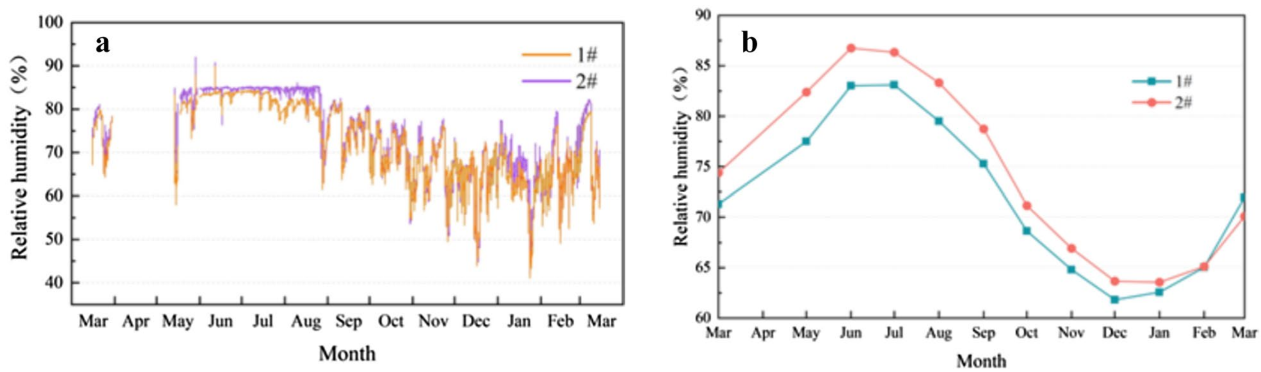

Fig. 7 Relative humidity variations at the different measurement points: **a** Relative humidity variations in one year; **b** monthly average relative humidity variations

Wall temperature monitoring data

In this paper, the wall temperature inside the male chamber of Yang Can's tomb was monitored from 7–8 March 2023 at different heights and depths of entry. Wall temperature data over the monitoring period are listed in Table 2. Table 3 provides the sunrise and sunset schedules for the period of 7–8 March 2023.

Monitoring data at different heights and at the same depth As shown in Fig. 8a, the overall trend in the wall temperature variations at the different heights remained consistent: the larger the height from the ground, the higher the wall temperature is; conversely, the smaller the height from the ground, the lower the wall temperature is. This occurs because cold air is denser than warm air and becomes concentrated in the lower part of the chamber. Therefore, the temperature in the lower part of the chamber is slightly lower than that in the higher part, and the wall temperature is correspondingly lower.

Monitoring data at different depths and the same height As shown in Fig. 8b, the variation range of the wall temperature at measurement point #1 was slightly greater than that at measurement point #2. This occurs because the point at a small depth is more notably affected by outdoor meteorological factors and therefore exhibits a slightly larger variation range. The temperature remains more constant at a large depth than at a small depth.

Test results

Sandstone density

The test data of the wax sealing method are listed in Table 4.

Table 2 Wall temperature monitoring data

Time		Measurement point #1 wall temperature (℃)			Measurement point #2 wall temperature (℃)		
		High	Middle	Low	High	Middle	Low
2023.3.7	1:40	9.6	9.4	9.1	9.9	9.4	9.2
	3:40	9.5	9.4	9.1	9.6	9.5	8.9
	5:40	9.4	9.3	9.1	9.6	9.4	9.1
	7:40	9.4	8.9	8.4	9.7	9.4	9
	9:40	9.7	9.3	8.7	9.8	9.6	9.1
	11:40	10.1	9.5	8.9	9.9	9.6	9.5
	13:40	10.4	9.9	9.2	10.3	9.9	9.3
	15:40	10.6	10	9.5	10.7	10.1	9.5
	17:40	11.0	10.2	10	11.4	10.2	10.4
	19:40	10.7	10.1	9.8	11.3	10.1	10.1
	21:40	10.6	10.1	9.7	11	10.0	10
	23:40	10.5	9.9	9.6	10.7	10.0	9.8
2023.3.8	1:40	10.3	9.7	9.6	10.3	10	9.6
	3:40	10.2	9.7	9.3	10	9.8	9.5
	5:40	10.6	9.9	9.6	10.1	9.7	9.6
	7:40	10.1	9.3	9	9.2	9.6	9.4
	9:40	10.2	9.5	9.1	9.8	9.6	9.3
	11:40	10.7	10.2	9.4	10.3	10.3	9.5
	13:40	11	10.4	9.7	10.7	10.5	9.6
	15:40	11.2	10.5	9.9	10.8	10.6	10.1
	17:40	11.5	10.7	10.2	10.9	10.7	10
	19:40	10.9	10.5	10.2	10.7	10.6	10.2
	21:40	10.6	10.3	10.1	10.6	10.5	10
	23:40	10.5	10.3	10	10.6	10.4	10.2

Table 3 Timetable for sunrise and sunset during the tomb monitoring period in March 2023

Date	Sunrise	Midnoon	Sunset	Day length	Daybreak	Darkness
3.7	7:10:21	13:03:15	18:56:10	11:45:49	6:47:02	19:19:29
3.8	7:10:21	13:03:15	18:56:10	11:45:49	6:47:02	19:19:29

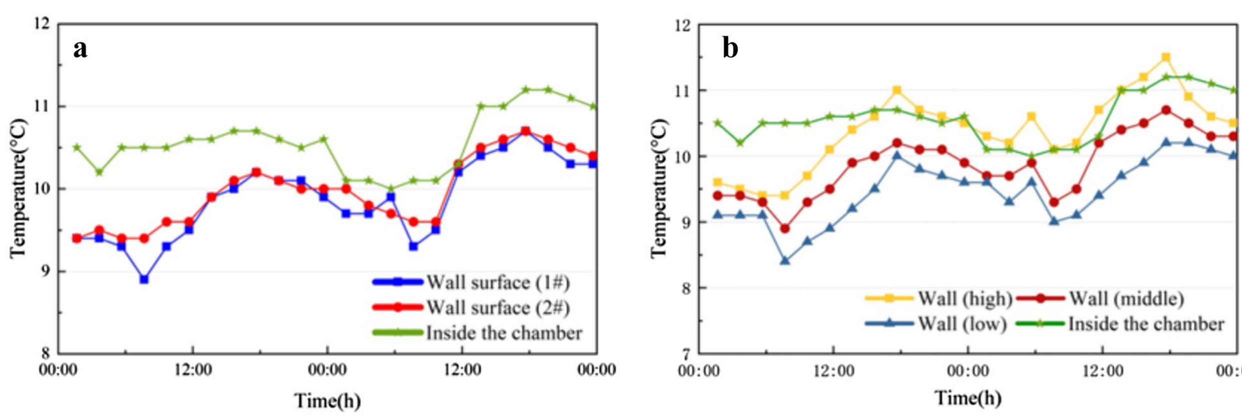

Fig. 8 Variation in the wall temperature: **a** At the different heights and the same depth of entry; **b** at the different depths and the same height

Table 4 Wax sealing test results

Test number	1	2	3
Rock mass (g)	42.71	45.35	42.50
Quality of the wax-sealed specimen (g)	46.21	47.31	47.90
Mass of the wax-sealed specimen in water (g)	24.85	26.70	24.37
Temperature of the body of water (°C)	24.10	24.10	24.10
Density of pure water (g/cm^3)	0.997	0.997	0.997
Density (g/cm^3)	2.41	2.44	2.40
Average density (g/cm^3)	2.42		

Moisture absorption test and isothermal moisture absorption and release curve

Moisture absorption test results Figure 9a shows the specimen after moisture absorption equilibrium is reached. In the five columns of the figure, the specimens (from left to right) are color-changing silica gel desiccant, a sandstone specimen with a particle size of R ≤ 1 mm, a sandstone specimen with a particle size of 1 mm < R ≤ 2 mm, a sandstone specimen with a particle size of 2 mm < R ≤ 5 mm, and a massive sandstone specimen. The air relative humidity for each row reached 97.6, 75.5, 59.1, 43.2, and 33.1%, respectively.

The variations in the equilibrium moisture content of the specimens with different particle sizes at different relative humidities are shown in a scatter plot (Fig. 9b). Notably, for the same particle size, the specimen equilibrium moisture content increased with increasing relative humidity.

Table 5 Isothermal moisture absorption and release curve equation model

Name	Model equation
Brunauer–Emmett–Teller (BET) [53]	$u = a\varphi/\left[(1-c\varphi)(1+b\varphi)\right]$
Oswin [54]	$u = a\left[\varphi/(1-\varphi)\right]^b$
Henderson [55]	$u = \left[\ln(1-\varphi)/a\right]^b$
Caurie [56]	$u = e^{a+b\varphi}$
Guggenheim–Anderson–de Boer (GAB) [57]	$u = \frac{abc\varphi}{(1-b\varphi)(1-b\varphi+bc\varphi)}$
Peleg [58]	$u = a\varphi^b + c\varphi^b$
Chen [59]	$u = a\varphi/(1-b\varphi)$

Isothermal moisture absorption and release curve The commonly adopted isothermal moisture absorption and release curve models are summarized in Table 5. The fitting coefficients a, b, c, and d have no physical meaning.

The fitting results showed that the Caurie model yielded the best fit, with R^2 values of 0.9975, 0.9992, 0.9969, and 0.9967 for R ≤ 1 mm, 1 mm < R ≤ 2 mm, 2 mm < R ≤ 5 mm, and coarse particle sizes, respectively. The parameters of the isothermal moisture absorption and release equilibrium curves of the Caurie model for the sandstone specimens with different particle sizes are provided in Table 6.

Water vapor permeability coefficient

The results of the test data are shown in Table 7.

Liquid water diffusion coefficient

The results of the test data are shown in Table 8.

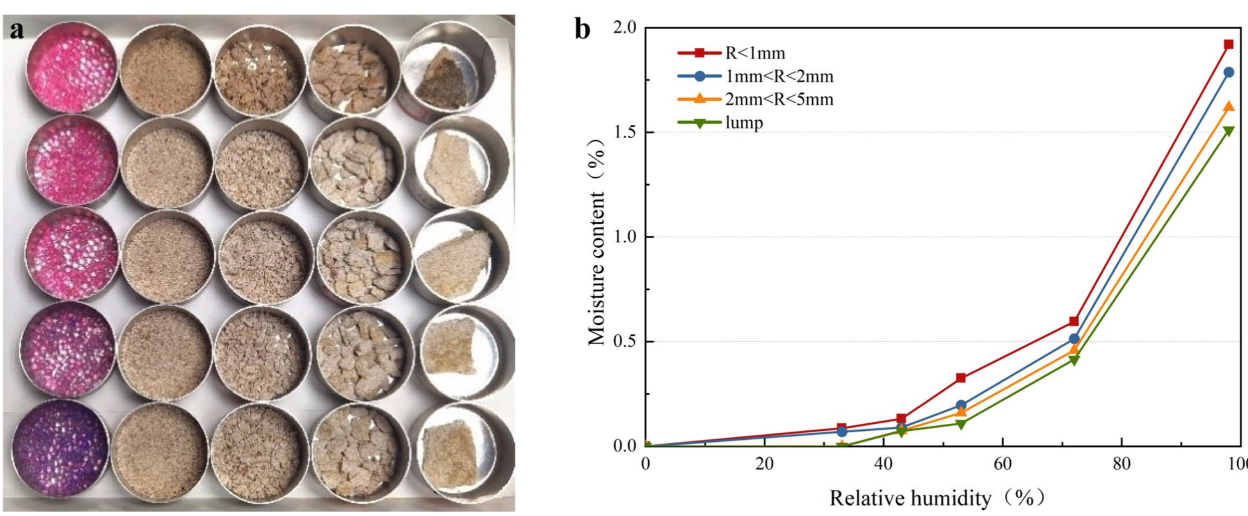

Fig. 9 Moisture absorption test results: **a** Specimen after the moisture absorption test; **b** effect of the particle size on the equilibrium moisture content

Table 6 Fitted parameters at 20 °C for the sandstone specimens with different grain sizes

Specimen size	a	b	R^2	Fitting function
R ≤ 1 mm	− 3.682	0.044	0.9968	$u = e^{-3.68+0.044\varphi}$
1 mm < R ≤ 2 mm	− 4.243	0.049	0.9992	$u = e^{-4.24+0.049\varphi}$
2 mm < R ≤ 5 mm	− 4.541	0.051	0.9967	$u = e^{-4.54+0.051\varphi}$
Coarse	− 4.807	0.053	0.9967	$u = e^{-4.81+0.053\varphi}$

As shown in Fig. 10, the intersection of the two fitted curves is (10.4105, 0.5149). The calculated liquid water diffusion coefficient of the specimens is $D_t = 4.49 \times 10^{-6}$.

Thermal conductivity

The results of the test data are shown in Table 9.

Simulation results

Validation of the simulation reliability

To evaluate the accuracy of the model in simulating complex chamber environments, the model-calculated simulation results were compared to the measurement data. Since the data of the measurement points at the different depths were basically the same, only the data from measurement point #1 were chosen for comparison, and the results are shown in Fig. 11.

The comparison chart reveals that the simulation results were generally consistent with the measured values, and the trend in the simulated wall temperatures was basically consistent with that in the measurement

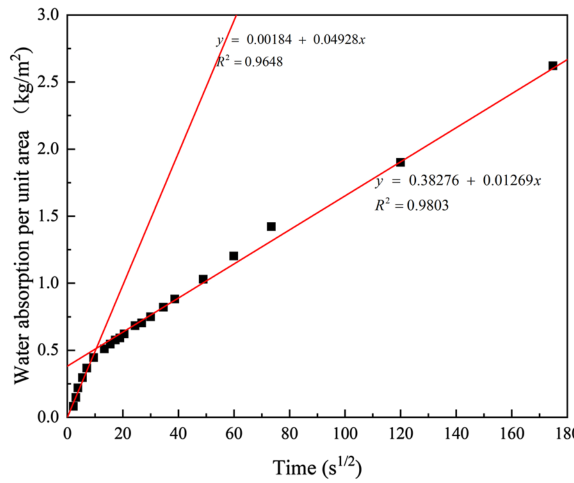

Fig. 10 Liquid water diffusion versus time

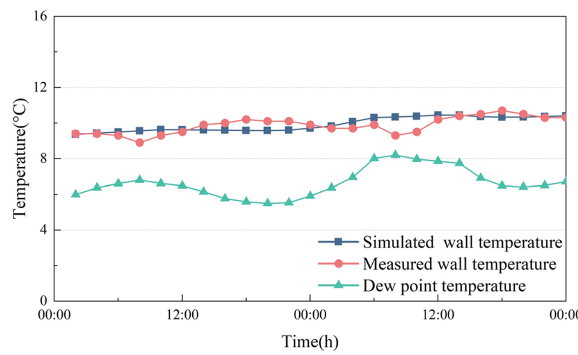

Fig. 11 Comparison of the simulated and measured wall temperatures of the tomb

Table 7 Test data for the water vapor permeability coefficient

Projects	Data
Mass variation Δm (g)	0.45
Specimen area A (m^2)	0.00196
Weighing interval Δt (s)	17,280
Saturated water vapor pressure at 20 °C P_s (Pa)	2337
Specimen thickness h (m)	0.01
Water vapor permeability coefficient $\delta_p\,[g/(Pa \times s \times m^2)]$	2.33×10^{-7}

Table 8 Raw liquid water diffusion volume test data

Time (t/s)	Mass (m/g)	Time (t/s)	Mass (m/g)	Time (t/s)	Mass (m/g)	Time (t/s)	Mass (m/g)	Time (t/s)	Mass (m/g)
0	123.40	50	124.12	300	124.53	900	124.87	5400	126.19
5	123.56	70	124.23	360	124.56	1200	125.01	14,400	127.13
10	123.69	100	124.31	420	124.62	1500	125.13	30,600	128.54
20	123.83	180	124.40	600	124.74	2400	125.42	/	/
30	123.98	240	124.47	720	124.78	3600	125.76	/	/

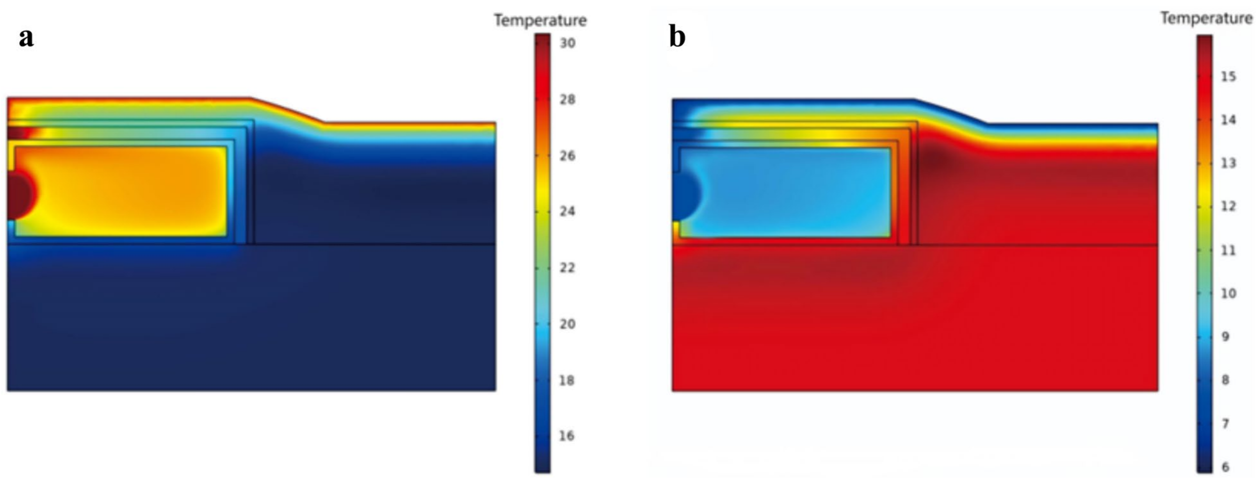

Fig. 12 Temperature distribution on a typical summer day and a typical winter day: **a** Typical summer day; **b** typical winter day

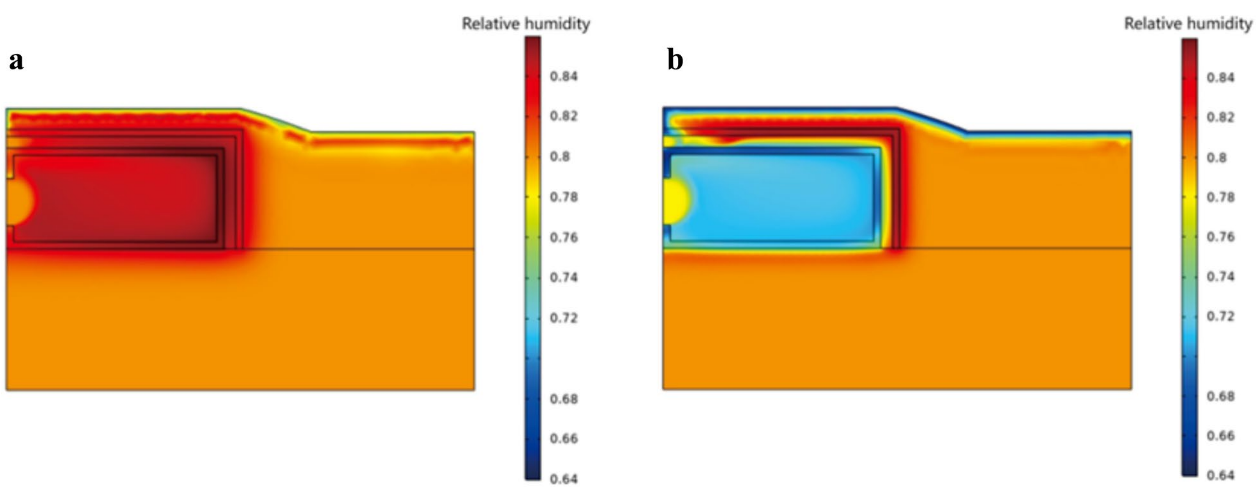

Fig. 13 Relative humidity distribution on a typical summer day and a typical winter day: **a** Typical summer day; **b** typical winter day

data, which is close to the average of the measured values. The simulated and measured values differed because the model was simplified, and it is reasonable that there was an error between the simulated and measured data. Therefore, the simulation results of the heat and humidity transfer computational fluid dynamics (CFD) airflow model of Yang Can's tomb can capture the heat and humidity migration processes inside the tomb relatively well, and the results are accurate and credible.

Table 9 Thermal conductivity parameters

Thermal diffusion coefficient	Heat conduction	Specific heat
$1.28 \times 10^{-6} m^2/s$	$2.54 W/(m \cdot K)$	$863 J/(kg \cdot K)$

Seasonal variation patterns

As shown in Figs. 12 and 13, in winter, the temperature of the walls of the chamber was higher than that of the

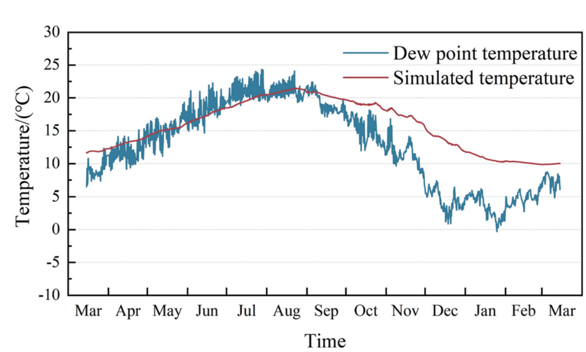

Fig. 14 Simulated wall temperature versus the dew point temperature

Table 10 Duration and proportion of water vapor condensation by month

Month	Days of condensation	Hours of condensation	Percentage of condensation hours
Mar	1	3	0.40%
Apr	13	106	14.25%
May	24	380	51.08%
Jun	28	496	66.67%
Jul	31	604	81.18%
Aug	21	289	38.84%
Sept	13	149	20.03%
Oct	0	0	0
Nov	0	0	0
Dec	0	0	0
Jan	0	0	0
Feb	0	0	0
Annual	126	2027	23.14%

air inside the chamber, which facilitates heat transfer from the walls to the air. In the summer months, the temperature of the walls of the chamber was lower than that of the air within the chamber, which promotes heat transfer from the air to the walls.

The above demonstrates that locations at greater depths and shallower heights from the ground exhibit lower temperatures and greater relative humidities, which are more susceptible to condensation phenomena and should receive increased attention. Therefore, the lower side of the rear wall surface of the chamber was selected as the study section to simulate the wall surface temperature variations. Based on the air temperature and humidity inside the chamber, the critical temperature at which water vapor condensation occurs, i.e., the dew point temperature, can be derived. Water vapor condensation occurred when the wall temperature of the chamber was lower than the dew point temperature. Moreover, when the wall temperature of the chamber remained lower than the dew point temperature for a period longer than 2 h, condensation risk occurred. As shown in Fig. 14, water condensation in the chamber occurred most severely in spring and summer. In contrast, water vapor condensation in the chamber in autumn and winter was less severe.

The simulation results were tabulated on a monthly scale, which provides a more intuitive overview of the severity of water vapor condensation inside the chamber of Yang Can's tomb. As indicated in Table 10, the total number of days with water vapor condensation throughout the year was 126, and the total duration was 2027 h; i.e., water vapor condensation could occur

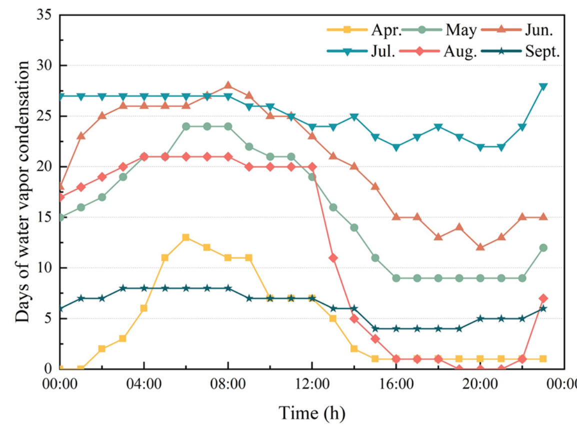

Fig. 15 Water vapor condensation during the different periods

on more than one-third of the total number of days and during more than 20% of the year, which is a clear indication of hazard. Throughout the year, water vapor was less likely to condense from October to February due to the low relative humidity inside the chamber. Water vapor condensation could begin at the end of March and could continue until early September. During the period with a risk of condensation, this phenomenon was more severe in May, June, July and August, with 2/3 of the days exhibiting a risk of condensation. Condensation was again most severe in July, with an almost daily risk of condensation. Notably, water vapor condensation occurred more than 80% of the time, which must be mitigated.

Daily variation patterns

Water vapor condensation varied at different times of the day. As shown in Fig. 15, water vapor condensation occurred mainly between 23:00 and 13:00, with a slightly smaller number of open-sky instances between 13:00 and 22:00. This occurs because of the low sunlight in the morning, coupled with a certain lag in the temperature variations inside the chamber relative to the outside environment. After 13:00, the temperature outside the chamber reached its daily peak, and the wall surface and air temperatures inside the chamber increased accordingly. However, the specific heat capacity of air is 1.005 kJ/(kg • K) (at a temperature of 300 K), which is higher than that of sandstone. Notably, the temperature of a material with a high specific heat capacity increases more slowly under the absorption of the same amount of heat, so the wall surface temperature changes faster than the air temperature inside the chamber. As a result, the wall temperature increased more rapidly than the air temperature inside the chamber, and condensation slightly improved. After sunset, the temperature gradually decreased, and the rate of wall surface temperature reduction was greater than that of air temperature reduction inside the chamber. When the wall surface temperature within the chamber was reduced to the dew point temperature, water vapor condensation started and persisted until the next day after 13:00, when the wall surface temperature became higher than the dew point temperature, and the condensation process stopped. As this process advances, the condensation disease continues to worsen.

Water vapor condensation mechanism and risk rating

Water vapor condensation mechanism

The physical process by which a given fluid is converted from a gaseous state to a liquid state with energy release is referred to as condensation. Both the attainment of saturated water vapor pressure and the presence of condensation nuclei are essential for water vapor condensation [60]. The wall surface of Yang Can's tomb comprises sandstone rock carvings, and the surface is relatively rough, combined with the long-term weathering effect. Weathered powder and dust are attached to the surface of the rock wall, providing countless condensation nuclei for water vapor condensation. Condensation nuclei can mainly be divided into water-soluble and water-insoluble condensation nuclei, of which the surface can be wetted by water. The relative humidity needed for condensation of the latter is more than 100%. The relative humidity in Yang Can's tomb does not exceed 100%, so water vapor condensation is related only to water-soluble condensation nuclei.

Saturated water vapor pressure (SWVP)

The saturated water vapor pressure refers to the pressure at which water vapor is saturated. According to Tetens' model [61], the saturated water vapor pressure can be obtained as:

$$e_w(T) = e_w(0) \times 10^{\frac{aT}{b+T}} \tag{1}$$

where $e(T)$ is the actual partial pressure of water vapor at an air temperature of T (hPa); $e_w(T)$ is the saturated water vapor pressure at an air temperature of T (hPa); $e_w(0)$ is the saturated water vapor pressure at a temperature of 0 °C; and T is the air temperature (℃).

Relative humidity

The relative humidity (RH) is the ratio of the partial pressure of water vapor actually contained in the air to the saturated water vapor pressure at the same temperature. The relative humidity is dimensionless but can be expressed as a percentage. This parameter can be obtained by Eq. (2):

$$RH = \frac{e(T)}{e_w(T)} \times 100\% \tag{2}$$

where RH is the relative humidity of air and the remaining physical quantities are the same as those above.

Dew point temperature (DP)

The dew point temperature is the temperature at which water vapor in the air cools to saturation, i.e., the critical temperature at which water vapor condenses on solid surfaces. The dew point temperature cannot be directly obtained from observations but can be converted from the saturated water vapor pressure by an empirical equation. The dew point temperature can be calculated by Eqs. (3) to (9).

$$RH = \frac{e(T)}{e_w(T)} \times 100\% = 100u \tag{3}$$

$$u = \frac{e(T)}{e_{sat}(T)} = \frac{e_{sat}(DP)}{e_{sat}(T)} \tag{4}$$

Substituting Eq. (1) into Eq. (4) yields the following:

$$u = \frac{e_{sat}(DP)}{e_{sat}(T)} = \frac{e_{sat}(0) \times 10^{\frac{aDP}{b+DP}}}{e_{sat}(0) \times 10^{\frac{aT}{b+T}}} = 10^{\left(\frac{aDP}{b+DP} - \frac{aT}{b+T}\right)} \tag{5}$$

$$logu = \frac{aDP}{b+DP} - \frac{aT}{b+T} \tag{6}$$

$$DP = \frac{b+DP}{a} logu + \frac{b+DP}{a} \cdot \frac{aT}{b+T} \approx \frac{b+T}{a} logu + T \tag{7}$$

In the above equations:

$$logu = log\left(\frac{RH}{100}\right) = logRH - 2 \tag{8}$$

When the air temperature is 0 °C, for the saturated water vapor pressure on a horizontal plane, a = 7.5 and b = 237.3 °C. Therefore, the dew point temperature can be expressed as follows (9):

$$DP = \frac{273.3 + T}{7.5}\left(logRH - 2\right) + T \tag{9}$$

The dew point temperature can be calculated for different air temperatures and humidities using Eq. (9).

Physical model of water vapor condensation

By comparing the wall temperature inside the chamber with the corresponding dew point temperature, it can be determined whether condensation occurs. When the wall temperature inside the chamber falls below the dew point temperature, water vapor condensation begins. Condensation first occurs in wall cracks and pores, and once droplets are generated on the wall, water vapor condensation ensues at the gas–liquid partition surface. Therefore, in this section, both condensation within pores and condensation on the rock surface are considered.

Condensation in pores Humid air in contact with porous materials contains water vapor that can be transferred through the material pores, and when the temperature of the porous material is lower than the dew point temperature, water vapor condensation occurs within the pores. The temperature and water vapor distributions in porous materials determine whether water vapor condensation occurs, and the conditions needed for water vapor condensation are more likely to be achieved at locations with lower temperatures and higher relative humidities. When condensation water is present in the pores of a given material, the material exhibits a wet state, and the material thermal conductivity increases, which further contributes to condensation. The water vapor condensation process in the different parts of the pore space can be divided into condensation in the open pore space and condensation in the internal pore space.

Surface condensation When water vapor in humid air comes into contact with a cold solid surface (exhibiting a temperature below the saturation temperature), it condenses on the surface to form liquid water. There are usually two mechanisms of water vapor condensation on solid surfaces: film condensation and droplet condensation (Fig. 16). If the produced condensation water wets the wall surface, i.e., the solid–liquid contact angle is high, film condensation occurs. Conversely, droplet condensation occurs. The contact angle of the sandstone surface of Yang Can's tomb is less than 90°, so film condensation occurs on the tomb wall.

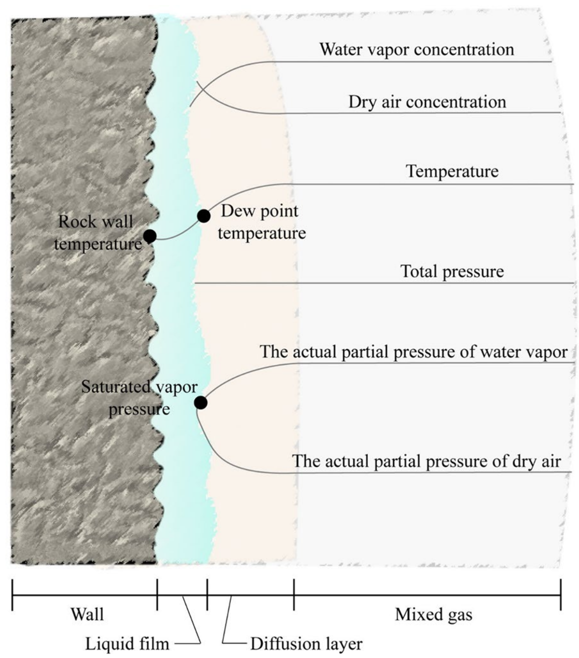

Fig. 17 Physical model of water vapor condensation on cave walls

A model of condensation on the sandstone surface inside the chamber is shown in Fig. 17. A mixture of air containing noncondensable gases (dry air) and water vapor with a certain temperature and humidity enters the chamber from the outside and reaches the vicinity of the chamber walls. When the wall temperature inside the chamber is lower than the dew point temperature of the air near the wall, the water vapor contained in the air

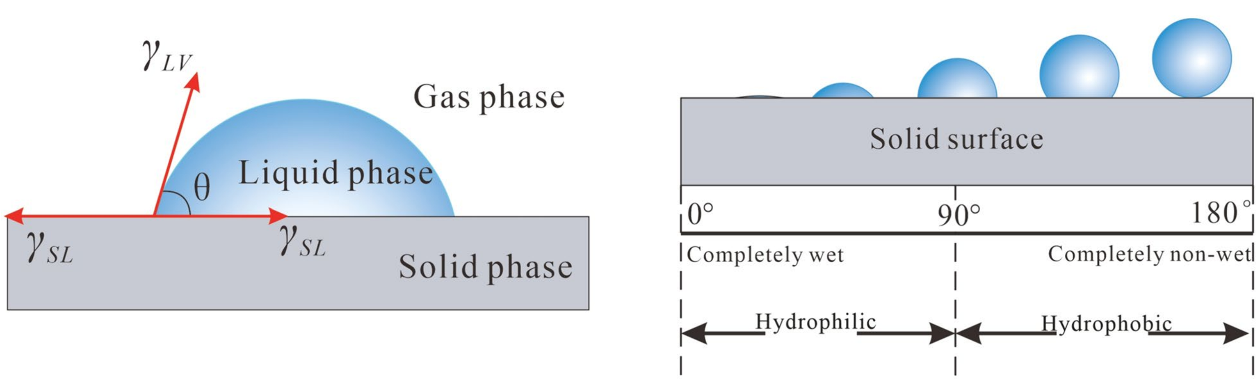

Fig. 16 Diagram of the contact angle and the corresponding wetting state

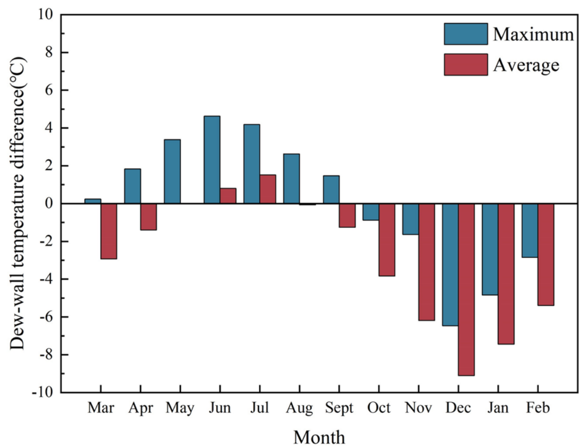

Fig. 18 Statistics of the dew–wall temperature difference by month

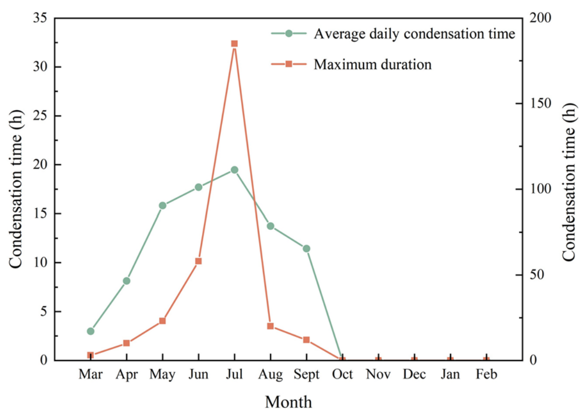

Fig. 19 Statistics of the condensation time by month

condenses into liquid water, forming a liquid film on the wall that separates the humid air from the wall. There is a high-concentration noncondensable gas diffusion layer at the interface between the liquid film and humid air, in which water vapor continuously undergoes condensation mass and heat transfer processes, as well as changes in the amount of heat flowing between the gas and liquid phases. Notably, the noncondensable gas diffusion layer is gradually entrained into the main flow with increasing condensation depth.

In the process of water vapor condensation, the total pressure of the humid air near the rock wall remains constant, while the water vapor partial pressure decreases as the humid air passes through the noncondensable gas diffusion layer, reaching the saturated water vapor pressure at the liquid film interface. The actual partial pressure of dry air continues to increase. Water vapor continues to condense into liquid water, resulting in a gradual decrease in the water vapor concentration in humid air and a subsequent increase in the water vapor concentration in dry air. As humid air passes through the noncondensable gas diffusion layer, the occurrence of resistance generates energy loss, causing the temperature to continuously decrease, while water vapor condensation at the wall surface continuously releases heat, causing a slight increase in the temperature of the rock wall. As condensation continues, equilibrium is eventually reached. The thickness of the liquid film gradually increases, and excess liquid water flows down the wall.

Condensate risk rating

To better prevent and manage water vapor condensation in Yang Can's tomb and to quantify condensation on a monthly scale, the dew–wall temperature difference, i.e., the difference between the dew point temperature and the wall temperature, was introduced. Figure 18 shows statistics of the dew–wall temperature difference for each month of the year, with a larger dew–wall temperature difference indicating a greater risk of condensation. As shown in Fig. 18, there was no risk of condensation from October to February when the dew–wall temperature difference was less than 0 °C. From May to August, a high risk of condensation occurred.

Figure 19 shows the statistics of the condensation duration for each month of the year. Notably, the longer the condensation duration is, the greater the amount

Table 11 Water vapor condensation classes

Water vapor condensation class	Dew–wall temperature difference and duration	Description of the water vapor condensation risk and countermeasures
I	Dew–wall temperature difference less than 0 °C	*Low risk*; no need for control measures, focus on the dew–wall temperature difference
II	Dew–wall temperature difference of 0–2 °C, with a condensation duration not exceeding 12 h	*Medium risk*; immediately implement condensation prevention and control measures and closely monitor the variations in the dew–wall temperature difference
III	Dew–wall temperature difference greater than 2 °C or condensation lasting more than 12 h	*High risk*; immediately implement all condensation control measures to prevent the situation from worsening

of condensation water and the greater the damage to artifacts. A comparison of Figs. 21 and 22 revealed that when the dew–wall temperature difference was less than 2 °C, the condensation duration did not exceed 12 h. When the dew–wall temperature difference was large, the condensation duration was also longer, and there was a high risk of condensation. For example, the maximum dew–wall temperature difference in July was 4.18 °C, while the maximum duration of water vapor condensation was 185 h, which is extremely harmful. Throughout the year, the condensation duration exceeded 30% of the total duration, with May to August exhibiting the highest incidence of water vapor condensation, mostly in June and July. During the day, a high incidence of water vapor condensation occurred from the morning to 13:00, but condensation problems during the remainder of the day should not be underestimated.

Through the above analysis, the severity of water vapor condensation was classified into three levels, as summarized in Table 11. This study provides a reference basis for managing water vapor condensation in Yang Can's tomb.

Condensation control measures

According to a previous study, the period of most severe water vapor condensation in Yang Can's tomb is summer, and the occurrence of condensation disease is related to the wall temperature and the air temperature and humidity conditions. Therefore, preventive measures for water vapor condensation mainly include increasing the wall temperature and reducing the ambient humidity. However, due to the unique nature of cultural relic protection, the use of light and heat to increase the wall temperature may cause increased relic weathering, so reducing the relative humidity within the chamber was primarily considered in this paper. There are two ways to reduce the relative humidity inside the chamber, either by allowing water vapor to escape through the chamber opening or by direct drying within the chamber.

Expel water vapor from the chamber opening

Accelerated air circulation

Based on the above study, the greater the depth of the chamber is, the greater the relative humidity and the more serious the condensation phenomenon, which occurs because of the poor air mobility in areas at greater depths. To accelerate air circulation both inside and outside the chamber, the chamber should first be moderately ventilated. When the relative humidity inside the chamber is high, active ventilation can be employed, thus lowering the dew point temperature inside the chamber and alleviating condensation. In winter, the relative humidity inside the chamber is much lower than that outside the chamber, and it is advisable to close the chamber door to prevent water vapor from entering the chamber. In summer, the relative humidity inside the chamber is greater than that outside the chamber, and the chamber door should be opened to discharge humid air from inside the chamber. In addition, air exchange devices can be added at locations with large burial chamber depths where the ventilation effect is poor. For example, a fan can be installed to accelerate the air flow rate at large depths, and the airflow direction within the chamber can be adjusted at the same time.

Reducing the temperature difference between the inside and outside of the chamber

Diffusive movement of water vapor always occurs from high to low water vapor pressures and from high to low temperatures. The temperature inside the chamber is lower than that outside the chamber in summer, so water vapor moves from outside to inside the chamber. Therefore, the temperature difference between the inside and outside of the chamber should be reduced in summer, including increasing the temperature inside the chamber and decreasing the temperature outside the chamber to inhibit water vapor movement into the chamber. Raising the temperature inside the chamber may increase the dew–wall temperature difference, resulting in condensation and possibly causing damage to the artifacts. Lowering the temperature outside the chamber suggests lowering the temperature of a section of space outward from the chamber opening to serve as a buffer between the inside and outside environments of the chamber. There is no shelter outside the burial chamber, and direct sunlight in summer increases the temperature of the bluestone pavement outside the burial chamber. Consideration can be given to planting trees on both sides of the bluestone pavement at the entrance of the burial chamber or building eaves at the entrance of the burial chamber to provide a certain degree of shading effect and reduce the temperature at this location.

Remove moisture inside the chamber

Desiccant dehumidification

In this paper, a color-changing silica gel desiccant was selected for the moisture absorption balance test. Color-changing silica gel particles exhibit notable adsorption, and moisture absorption is a physical process in which the particles do not react with water to generate toxic substances. Moreover, the process cost is low, and the particles can be reused after drying. Notably, moisture absorption can be assessed according to the color of the particles.

Dehumidifier dehumidification

Considering the large amount of desiccant used and the need for frequent replacement, which increases the labor cost, dehumidifiers can be used instead to directly reduce the air relative humidity inside the chamber. Dehumidified air flows through the fan, and humid air is pumped into the machine inside. Through heat exchange, water vapor in the humid air condenses into liquid water, and dry air is then discharged from the machine. With a continuous cycle, the relative humidity of the indoor air can be reduced. At present, dehumidifiers for preventing and controlling water condensation have been widely used in the field of stone cultural relic protection. In the Yungang Grottoes, two mausoleum crypts of the South Tang Dynasty were equipped with dehumidifiers, with satisfactory performance.

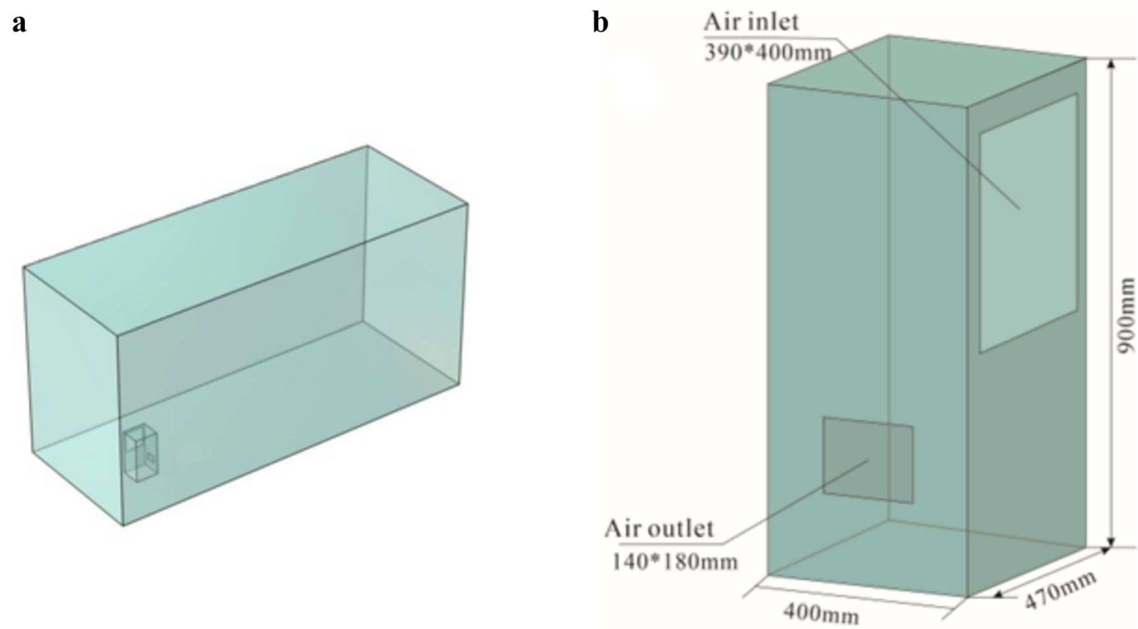

Fig. 20 Dehumidification model: **a** Dehumidification programmed model; **b** physical model of the dehumidifier

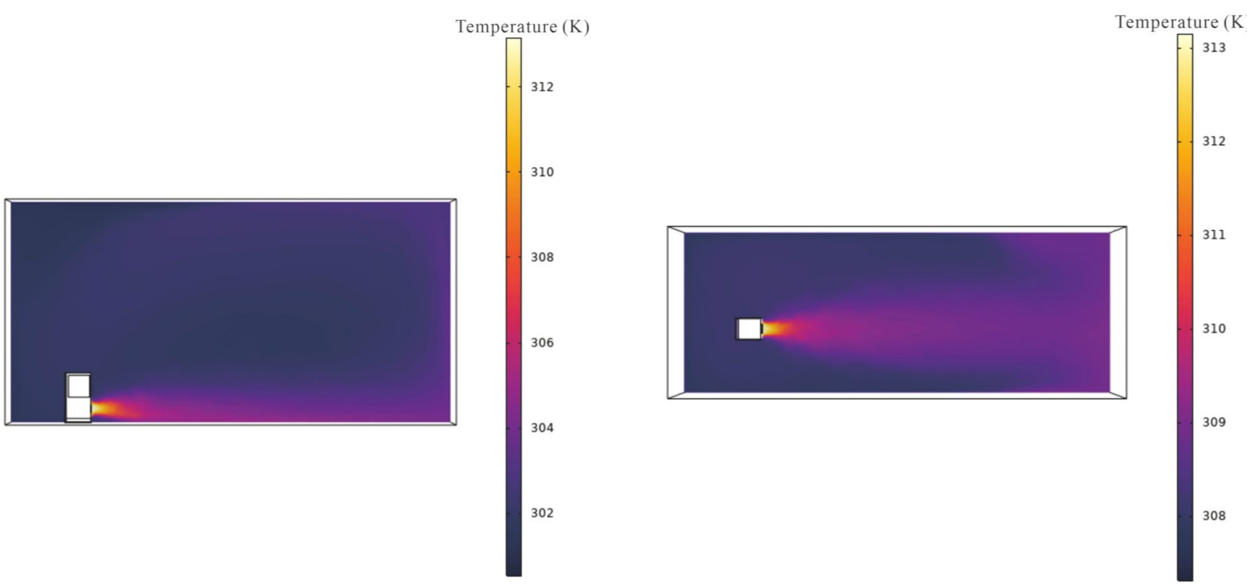

Fig. 21 Air temperature distribution in the dehumidifier air supply outlet cross section

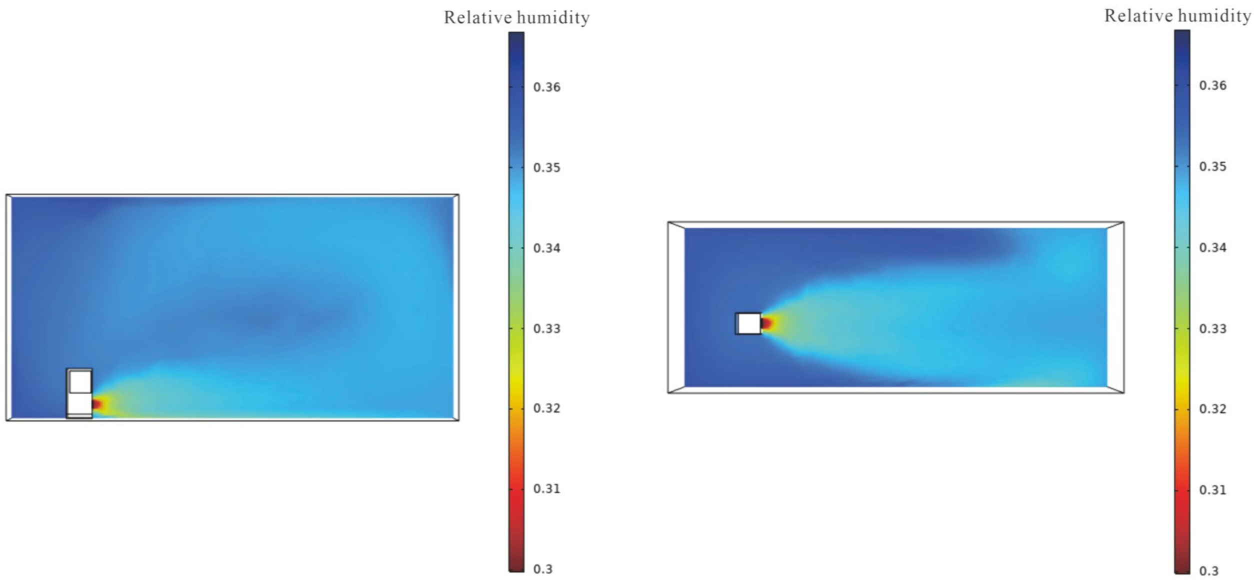

Fig. 22 Air relative humidity distribution in the dehumidifier air supply outlet cross section

Dehumidification effect simulation

In this paper, the temperature and humidity inside the chamber of Yang Can's tomb after dehumidifier installation were simulated to provide a theoretical basis for water condensation prevention and control in Yang Can's tomb.

To reduce the computational effort, it was assumed that the door of the chamber remained closed, and the chamber was treated as a closed area, ignoring air exchange with the outside. Moreover, the previous analysis indicated that the most severe water vapor condensation inside the chamber occurred in July, so the initial temperature and humidity inside the chamber were set to the average air temperature and humidity, respectively, inside the chamber in July, i.e., the air temperature is 24 °C and the relative humidity is 84%. The wall surface inside the chamber was regarded as a thermal and humidity insulation boundary. The boundary conditions of the dehumidifier were set to an air velocity of 5.1 m/s at the air supply outlet, a supply air temperature of 313.15 K, and a supply air relative humidity of 30.3% (Fig. 20).

Figures 21 and 22 show that through dehumidifier use for treating dry, high-temperature air and the surrounding humid, low-temperature air, heat and moisture transfer constantly occurred at the outlet with the highest temperature and the lowest relative humidity. Along the direction of the outlet, the temperature gradually decreased, and the humidity gradually increased. At 20 min after dehumidifier activation, the relative humidity inside the chamber was theoretically reduced from 84% to a maximum of 36%, and the temperature inside the chamber was increased from 24 °C to a minimum of 28 °C. The dehumidifier was then deactivated, and the relative humidity was reduced to a maximum of 36%. Based on the simulation results, it could be concluded that the dehumidifier could reduce the ambient relative humidity inside the chamber and lower the dew point temperature, thus inhibiting water vapor condensation inside the chamber. Moreover, the figures reveal that the relative humidity near the wall facing away from the outlet was greater than that near the wall facing the outlet, and under the actual conditions of Yang Can's tomb, there was no completely closed state even if the door of the tomb was closed. Therefore, in practice, more time may be needed for obtaining the simulated dehumidification effect than the time required to reach the preset relative humidity because the dehumidification effect near the wall at the back of the dehumidifier outlet is slightly worse. The greater the depth inside the chamber and the smaller the height from the ground, the more severe the water vapor condensation phenomenon is. Therefore, during the actual use of dehumidifiers, the air outlet of the dehumidifier should be directed toward the rear wall of the chamber to reduce the relative humidity within the chamber at a large depth and to inhibit condensation.

Discussion

The above measures are based on the results of on-site monitoring, indoor tests and software simulations.

Therefore, their accuracy and effectiveness are influenced by numerous factors.

Choice of measurement devices and instruments

First, the concealment of the instruments and equipment should be considered to ensure that they do not affect the visiting experience of tourists. Second, the precision should be considered, and the accuracy of the monitoring data should be ensured by choosing the appropriate precision for monitoring. Finally, the long-term stability of the equipment should be considered, especially for long-term monitoring. Regarding the equipment selected in this paper, the above points were considered, but in April and May, equipment upgrades were not recorded. In subsequent studies, these data should be improved.

Choice of days for data recording at the site

The number of days of data recording is mainly determined from the perspective of whether measurement will cause interference and influence cultural relics. In the case of not severely impacting the artifacts and facilitating monitoring, the number of days of data recording is sufficient. For example, in a previous study on monitoring the temperature and humidity inside and outside a chamber, data were recorded throughout the year [52]. In the case of possible impacts on the artifacts, a representative number of days should be selected for data recording, such as the measurement of the wall temperature.

Absence or presence of the influence of solar irradiation on the air mass in front of the tomb entrance

In a previous study, it was found that the temperature change trend outside the tomb of Yang Can's tomb is basically consistent with the change in the total irradiation, indicating that irradiation is a direct factor leading to atmospheric change outside the tomb. The temperature inside the tomb is less affected by irradiation, and the change is smaller and more stable overall. Notably, the amount of solar irradiation and the temperature inside and outside the burial chamber exhibit seasonal characteristics. In fall and winter, the irradiation amount is smaller, so the temperature inside and outside the chamber shows a decreasing trend; in spring and summer, the irradiation amount is greater, and the temperature inside and outside the chamber exhibits an increasing trend [52].

Presence of visitors

In monitoring the temperature and humidity inside the tomb throughout the year, the access of tourists impacts the monitoring results, but this impact can be ignored because of the long monitoring cycle. In monitoring the wall surface temperature, due to the limitations of the distance between the visitors and wall surface and the short measurement time of the infrared equipment, the impact of visitor access on the monitoring results can also be ignored.

Conclusion

In this paper, the water vapor condensation mechanism in Yang Can's tomb was systematically investigated through the combination of on-site monitoring, indoor experiments and software simulations. In the investigation, the following conclusions could be obtained:

1) The magnitudes of the temperature and humidity variations at the different measurement points inside the chamber basically remained the same throughout the day, but the greater the depth was, the poorer the air circulation and the higher the relative humidity. Additionally, the locations at greater depths exhibited slightly higher temperatures in winter and slightly lower temperatures during the other seasons.
2) The temperature and humidity distributions inside the chamber were simulated, and it was concluded that a high incidence of water vapor condensation was observed from April to September, and the condensation time accounted for more than 90% of the total time.
3) Starting from the relevant concepts of condensation and a physical model of wall condensation, the phenomenon of water vapor condensation and its principles were analyzed in depth, and a physical model of water vapor condensation was established. According to the concept of the dew point temperature, when the wall temperature of the chamber is lower than the dew point temperature, water vapor starts to condense.
4) Water vapor condensation hazard classification criteria based on Yang Can's tomb, which can be assessed by the dew–wall temperature difference and condensation duration, were proposed. The risk of water vapor condensation can be classified into three categories: high, medium and low.
5) Measures were proposed for preventing water vapor condensation damage in Yang Can's tomb, which can be achieved by increasing the wall temperature and reducing the ambient humidity.

Acknowledgements
We thank our colleagues at Northwest Research Institute Limited Company of China Railway Engineering Corporation for their great help in this work. We thank the editors for their patience processing our manuscript. The anonymous reviewers are gratefully acknowledged for their careful and insightful reviews.

Author contributions
Conceptualization, PL and BS; methodology, WS and XX; validation, WS; formal analysis, YL, XX. and Q.W; investigation, YL and CL; writing—original draft preparation, WS and XX; writing—review and editing, PL and BS; funding acquisition, PL and BS. All authors have read and agreed to the published version of the manuscript.

Funding
This work was supported by the National Natural Science Foundation of China (No. 42267023 and No. 51408285), the Natural Science Foundation of Gansu Province (No. 20JR5RA293), the Fundamental Research Funds for the Central Universities (No. lzujbky-2021-57), the Science and Technology Item Foundation of Northwest Research Institute Limited Company of CREC, the Education Science and Technology Innovation Project of Gansu Province and the Education Reform Research Project of Lanzhou University.

Data availability
The authors confirm that the data supporting the findings of this study are available within the article.

Declarations

Competing interests
Author Bo Sun was employed by the China Railway Cultural Heritage rehabilitation Technology Innovation Co., Ltd. of C.R.E.C. The remaining authors declare that the research was conducted in the absence of any commercial or financial relationships that could be construed as a potential conflict of interest.

Received: 1 April 2024 Accepted: 22 May 2024
Published online: 03 June 2024

References

1. Shi JZ. Yang Can 's tomb in Zunyi. Contemp Guizhou. 2007;(07):52.
2. Reynolds O, Roscoe HEI. On the condensation of a mixture of air and steam upon cold surfaces. Proc R Soc Lond. 1997;21(139–147):274–81.
3. Monteith JL. Dew. Q J R Meteorol Soc. 1957;83(357):322–41.
4. Zheng RA. Sandy condensate characterizations. Acta Pedologica Sinica. 1963;11(1):84–91.
5. Jiang Q, Wang FK, Zhang WJ. Studies on sandy condensate and its role in water balance. Arid Zone Res. 1993;2:1–9.
6. Fang J, Ding YJ. An experimental observation of the relationship between sandy soil condensation water and micrometeorological factors in the arid desert region. J Desert Res. 2015;35(5):1200–5.
7. Garrecht H, Kropp J, Hilsdorf HK. Analysis of moisture protection in historic building. Ireland: The 8th International Brick and Block Masonry Conf; 1988. p. 1682–92.
8. Ludwig, N., Rosina, E. Moisture detection through thermographic measurements of transpiration. In: Proceedings of SPIE—The international society for optical engineering. 1997; Vol. 3056, pp 78–86.
9. Zhang HM, Ma GD, Su BY. A discussion of the treatment of water-seepage disease of the stone carvings in the Yungang Grotto near Datong. Hydrogeol Engin Geol. 2004;2004(05):64–7.
10. Sandrolini F, Franzoni E. An operative protocol for reliable measurements of moisture in porous materials of ancient buildings. Build Environ. 2006;41(10):1372–80.
11. Valentini M, Capitani D, Soroldoni L, Rosina E, Proietti N, Casellato U, Gobbino M. An integrated study for mapping the moisture distribution in an ancient damaged wall painting. Anal Bioanal Chem. 2009. https://doi.org/10.1007/s00216-009-3170-5.
12. Mahdavinejad M, Javanroodi K, Rafsanjani LH. Investigating condensation role in defects and moisture problems in historic buildings. case study: Varamin friday mosque in Iran. World J Sci Technol Sustain Dev. 2013;10(4):308–24.
13. Franzoni E, Bandini S, Graziani G. Rising moisture, salts and electrokinetic effects in ancient masonries: from laboratory testing to on-site monitoring. J Cult Herit. 2014;15(2):112–20.
14. Al-Omari A, Brunetaud X, Beck K, Al-Mukhtar M. Effect of thermal stress, condensation and freezing-thawing action on the degradation of stones on the castle of chambord. Fr Environ Earth Sci. 2013;71:3977–89.
15. Hoła A. Measuring of the moisture content in brick walls of historical buildings—the overview of methods. IOP Conf Ser Mater Sci Eng. 2017;251:012067.
16. Huang JZ, Wang JH, Gao F, Wang FR, Qi Y, Liu SJ. Recent progresses in sandstone cave temples conservation: a case study of yungang grottoes. Southeast Cult. 2018;01:15–9.
17. Rosina E. When and how reducing moisture content for the conservation of historic building. a problem solving view or monitoring approach? J Cult Herit. 2018;31:S82–8.
18. Sato M, Hattanji T. A laboratory experiment on salt weathering by humidity change: salt damage induced by deliquescence and hydration. Prog Earth Planet Sci. 2018. https://doi.org/10.1186/s40645-018-0241-2.
19. Freimanis R, Vaiskunaite R, Bezrucko T, Blumberga A. In-situ moisture assessment in external walls of historic building using non-destructive methods. Environ Clim Technol. 2019;23(1):122–34.
20. Liu S, Bai XY, Zhang B, Zhang ZJ, Sun JZ, Yang WF. Cause analysis and control measures of water damages in guihai's stone inscription. Hydrogeol Engin Geol. 2020;47(02):126–33.
21. Giaccone D, Santamaria U, Corradi M. An experimental study on the effect of water on historic brickwork masonry. J Cult Herit. 2020;3(1):29–46.
22. Vogel T, Dusek J, Dohnal M, Snehota M. Moisture regime of historical sandstone masonry—a numerical study. J Cult Herit. 2019. https://doi.org/10.1016/j.culher.2019.09.005.
23. Cabrera V, Yustres N, López-Vizcaíno R, Merlo S, Navarro V. Determination of the hygric properties of the heritage stone of the cathedral of cuenca through the water absorption by capillarity test. J Cult Herit. 2020. https://doi.org/10.1016/j.culher.2020.11.009.
24. Pratiwi SN, Wijayanto P, Putri CA. Diagnosis of capillary rise in heritage building. IOP Conf Ser Earth Environ Sci. 2021. https://doi.org/10.1088/1755-1315/780/1/012076.
25. Proietti N, Calicchia P, Colao F, Simone SD, Tatì A. Data on mineral research detailed by researchers at national research council (CNR) (moisture damage in ancient masonry: a multidisciplinary approach for in situ diagnostics). Min Miner. 2021. https://doi.org/10.3390/min11040406.
26. Luvidi L, Prestileo F, De Paoli M, Riminesi C, Manganelli Del Fà R, Magrini D, Fratini F. Diagnostics and monitoring to preserve a hypogeum site: the case of the mithraeum of marino laziale (Rome). Heritage. 2021;4(4):4264–88.
27. Hemeda S. Geotechnical modelling of the climate change impact on world heritage properties in Alexandria. Egypt Herit Sci. 2021;9(1):73.
28. Liu ZY, Dong ZJ, Zhou T, Cao LP. Water vapor diffusion models in asphalt mortar considering adsorption and capillary condensation. Constr Build Mater. 2021;308: 125049.
29. Ma C, Jiang XW, Yan HB, Zhou PY, Ren JG, Fan Y, Fan X, Wan L. A study of the formation pattern of condensation water in grottoes based on the infrared thermal imaging technology. Hydrogeol Engin Geol. 2022;49(04):30–6 (**In Chinese**).
30. Richards J, Brimblecombe P. The transfer of heritage modelling from research to practice. Herit Sci. 2022. https://doi.org/10.1186/s40494-022-00650-4.
31. Sass O, Viles H. Heritage hydrology: a conceptual framework for understanding water fluxes and storage in built and rock-hewn heritage. Herit Sci. 2022;10(1):66.
32. Zhang Y, Zhang YM, Huang JZ. Experimental study on capillary water absorption of sandstones from different Grotto heritage sites in China. Herit Sci. 2022;10(1):1–17.
33. Huang JZ, Zheng Y, Li H. Study of internal moisture condensation for the conservation of stone cultural heritage. J Cult Herit. 2022;56:1–9.

34. Zhang Y, Zheng Y, Huang JZ. Determination of water vapor transmission properties of sandstones in the yungang grottoes. Int J Archit Herit. 2022;18(3):357–69.
35. Zhou XH, Derome D, Carmeliet J. Analysis of moisture risk in internally insulated masonry walls. Build Environ. 2022;212: 108734.
36. Hoła A. Methodology of the quantitative assessment of the moisture content of saline brick walls in historic buildings using machine learning. Archiv Civ Mech Eng. 2023;23(3):141.
37. Yang HQ, Chen CW, Zhao G, Zhou JY. Electrical resistivity analysis for the internal capillary water migration mechanism of porous stone. Acta Geophys. 2023. https://doi.org/10.1007/s11600-023-01081-w.
38. Jaroš P, Vertaľ M, Slávik R. Hygric and thermal properties of slovak building sandstones. J Build Engin. 2023;66: 105891.
39. d'Ambrosio Alfano FR, Palella BI, Riccio G. Moisture in historical buildings from causes to the application of specific diagnostic methodologies. J Cult Herit. 2023;61:150–9.
40. de Oliveira LMG, Mesquita EFT, de Oliveira Freire FL, Bertini AA. The influence of the bricks and mortar characteristics, paint, and salts on the rising damp of historic masonries through hygrothermal simulation. J Cult Herit. 2023;64:92–101.
41. Sassu M, Puppio ML, Safabakhsh A. Damage and restoration of historical urban walls: literature review and case of studies. Frattura Ed Integrità Strutturale. 2023;17(65):194–207.
42. Daly P, Ninglekhu S, Hollenbach P, McCaughey JW, Lallemant D, Horton BP. Rebuilding historic urban neighborhoods after disasters: balancing disaster risk reduction and heritage conservation after the 2015 earthquakes in Nepal. Int J Disaster Risk Reduct. 2023;86: 103564.
43. Sun B, Li XY, Cui K, Hong J, Chen R, Jia C, Peng NB. Experimental study on the effects of hydrochemistry and periodic changes in temperature and humidity on sandstone weathering in the longshan grottoes. Herit Sci. 2023. https://doi.org/10.1186/s40494-023-01021-3.
44. Franzoni E, Berk B, Bassi M, Marrone C. An integrated approach to the monitoring of rising damp in historic brick masonry. Constr Build Mater. 2023;370: 130631.
45. Szemiot N, Hoa A, Sadowski U. Assessment of the effectiveness of secondary anti-damp insulation in heritage buildings made of historic brick the current state of knowledge research gaps and perspectives. Herit Sci. 2023. https://doi.org/10.1186/s40494-023-01043-x.
46. Yao SS, Yan ZF, Xu BK, Bi WB, Zhang JJ, Li H, Qu JH, Zhang SH. The influence of different clay/sand ratios on the hygrothermal properties of earthen plasters in the maijishan grottoes. Herit Sci. 2024;12(1):28.
47. Liu HL, Zhang Q, Zhang ZM, Guo QL, Lin WB, Gao WQ. Rainfall influence and risk analysis on the mural deterioration of dunhuang mogao grottoes. China Herit Sci. 2023;11(1):176.
48. Iskandar L, Bay-Sahin E, Martinez-Molina A, Toker Beeson S. Evaluation of passive cooling through natural ventilation strategies in historic residential buildings using CFD simulations. Energy and Buildings. 2024;308: 114005.
49. Sun B, Li XY, Cui K, Peng NB, Hong J, Chen R. Study on the characteristics of damaged sandstone in the longshan grottoes using water chemistry and freeze-thaw cyclin. Minerals. 2023;13(3):430.
50. Jr Allen Cooley L, Kandhal PS, Buchanan MS, Fee F, Epps A. Loaded wheel testers in the united states: state of the practice. Washington, D.C: Transportation Research Circular; 2000.
51. Zhao XF, Cao JY, Luo HF. Experimental study on measuring thermal properties of rock and soil with hot disk. China Meas Test. 2012;38(4):4.
52. Liu P, Shi WT, Sun B, Wang Q, Xie XK, Li CQ. Characteristics of the temperature and humidity variations of burial-type stone relics and a fitting model. Appl Sci. 2024;14(5):2157.
53. Brunauer B, Deming LS, Deming WE. Adsorption of gases in multimolecular layers. J Am Chem Soc. 1938;60(2):309–19.
54. Oswin CR. The kinetics of package life III the isotherm. J Chem Technol Biotechnol. 1946. https://doi.org/10.1002/jctb.5000651216.
55. Henderson SM. A basic concept of equilibrium moisture. Agric Eng. 1952;33:29–32.
56. Caurie M. A new model equation for predicting safe storage moisture level for optimum stability of dehydrated foods. Int J Food Sci Technol. 2007;5(3):301–7.
57. Berg CVD, Bruin, S. Water activity and its estimation in food systems. Water Act Influ. Food Qual. 1981;1–61.
58. Peleg M. Assessment of a semi-empirical four parameter general model for sigmoid moisture sorption isotherms1. J Food Process Eng. 1993;16(1):21–37.
59. Chen QG. Thermophysical theoretical basis for the design of underground cold storage buildings. J Refrig. 1980;03:30–46.
60. Gan XM. Study and control of condensation water in yungang grottoes. Beijing: China University of Geosciences Beijing; 2007.
61. Camuffo D. Microclimate for cultural heritage. Amsterdam: Elsevier; 1998.

Publisher's Note